Taylor & Francis
Taylor & Francis Group

IGNITION AND COMBUSTION CHARACTERISTICS OF NANOSCALE Al/AgIO$_3$: A POTENTIAL ENERGETIC BIOCIDAL SYSTEM

K. T. Sullivan,[1] N. W. Piekiel,[1] S. Chowdhury,[1] C. Wu,[1] M. R. Zachariah,[1,2] and C. E. Johnson[3]

[1]*Department of Mechanical Engineering, University of Maryland, College Park, MD, USA*

[2]*Department of Chemistry and Biochemistry, University of Maryland, College Park, MD, USA*

[3]*Chemistry and Materials Division, Naval Air Warfare Center, China Lake, CA, USA*

The authors investigated the ignition and reaction of Al/AgIO$_3$ thermites for potential use in biocidal applications. Rapid-heating wire experiments were performed to measure the ignition temperature and investigate the thermal decomposition of the oxidizer using a T-Jump/TOF Mass Spectrometer and an optical emission setup. Combustion experiments inside a constant-volume pressure cell were also carried out, and the relative performance was compared with other thermite systems. The ignition temperature in air at atmospheric pressure was found to be 1215 ± 40 K. The AgIO$_3$ was found to significantly outperform CuO and Fe$_2$O$_3$ oxidizers in pressurization tests, and this is attributed to the enhanced gas release as the AgIO$_3$ thermally decomposes to release iodine in addition to oxygen. The reacted product was collected to investigate the final state of the products. Transmission electron microscopy and X-ray diffraction were performed to show that the major Ag product species was AgI, and not elemental Ag and I$_2$. The AgI was found to be surface exposed to the environment, existing primarily as agglomerated spherical nanoparticles, and was found in some cases to coat the Al$_2$O$_3$ after the reaction.

INTRODUCTION

Interest in neutralizing biological-based weapons has posed a challenge to the use of traditional energetic materials that produce a very short-lived thermal event. It has recently been proposed that a new class of energetic material, which offers both a thermal event coupled with a long-lasting biocidal character, could be useful in mitigating biological materials. What really matters then is how much biocidal agent can be produced by the energetic, along with what chemical form it presents itself in the

final product. The latter point is particularly relevant because it is quite possible to have a biocidal product that either ends up to have a low surface area and thus minimal efficiency, or worse yet, be wrapped up within the matrix of one of the products of reaction and thus not exposed to the environment.

An ideal energetic system designed for neutralization of biological agents should possess the following characteristics:

1. High thermal release with minimal overpressure
2. The ability to produce a species that is effective against the biological agent, is nontoxic to humans, and also is chemically and thermally stable to keep it active for sustained periods of time.

For the thermal release component, reactive materials, particularly those comprising thermite chemistry, produce a very high energy release per unit volume or mass. Furthermore, because the products of combustion tend to be primarily in the condensed phase, some of the issues associated with high blast overpressures are minimized. For the biocidal component, a variety of materials could potentially be used, one of which is the subject of this work.

The highly insoluble salt, silver iodate ($AgIO_3$), has been considered recently for its potential use in thermite-based biocidal applications (Johnson et al., 2008). Silver exhibits biocidal properties in many forms (Rentz, 2003). Morones et al. (2005) investigated nanosized silver, and showed it to be effective at killing bacteria, especially when the particle size was very small (<10 nm). Smetana et al. (2008) also investigated the biocidal activity of several silver/silver-based samples with and without coatings and concluded that small, irregular surfaces are necessary for high biocidal activity. They claimed that silver ions are the actual biocidal species, and having silver oxide surfaces on the nanoparticles can serve to facilitate the transport of silver ions, and thus improve the effectiveness. Silver bromide nanoparticle/polymer composites have been reported to exhibit potent, long lasting antibacterial activity (Sambhy et al., 2006), and silver iodide is used as an antiseptic (Merck, 2001). Iodine is also a widely known and used biocide (U.S. Patent No. 7,033,509, 2006).

In the present work we investigated the burning of $Al/AgIO_3$ nanothermites, which are commonly classified as metastable intermolecular composites (MICs; Son et al., 2002). As discussed previously, we are concerned with both the combustion performance along with the final state of the products. Rapid-heating wire experiments and constant-volume combustion tests were performed in order to investigate the burning and report the ignition temperature. The reacted products were examined using X-ray diffraction and electron microscopy to determine the composition and morphology.

In discussing the performance of the $Al/AgIO_3$ system in this work, it often is helpful to make comparisons to two other common thermite systems, Al/CuO and $Al/Fe_2O_3 \cdot CuO$ is generally considered to be a relatively good oxidizer, whereas Fe_2O_3 is a relatively poor one, and we discussed some possible reasons for this in a recent work (Sullivan and Zachariah, 2010). It is necessary to include this data to provide some context for the measurements presented in this paper, in particular the combustion studies performed inside a pressure cell. The measurements we make

Table 1 Constant enthalpy and pressure thermodynamic equilibrium calculations of stoichiometric thermite systems. Data for Fe$_2$O$_3$ and CuO is taken from Fisher and Grubelich (1998). The AgIO$_3$ calculation was done using NASA's CEA equilibrium software with a constant enthalpy and pressure

Thermite reaction	mmol gas/g	Major gas species	Adiabatic temperature K	Comment
2Al + Fe$_2$O$_3$ → Al$_2$O$_3$ + 2Fe	1.4	Fe	3135	b.p. of Fe
2Al + 3CuO → Al$_2$O$_3$ + 3Cu	5.4	Cu	2843	b.p. of Cu
2Al + AgIO$_3$ → Al$_2$O$_3$ + Ag + I	∼8.9	Ag + I + Al$_2$O$_3$[a]	3681[b]	b.p. of Al$_2$O$_3$

[a]Al$_2$O$_3$ involves dissociation into several gaseous products (e.g., AlO, Al$_2$O, O, O$_2$), rather than molecular Al$_2$O$_3$.

[b]The product libraries do not contain some volatile species such as AlOI or AgI, and this may slightly affect the value.

are often relative in nature, and so we must show comparisons with materials tested under the exact same experimental conditions to give some idea of the relative performance.

Some thermodynamic equilibrium calculations of the thermites studied in this work are summarized in Table 1. Data for the Fe$_2$O$_3$ and CuO thermites were taken from Fischer and Grubelich (1998), with gas production based on adiabatic reaction at atmospheric pressure, and did not take into account the presence of an oxide shell on the Al. The Al/AgIO$_3$ equilibrium data were calculated using the NASA CEA software for constant enthalpy and pressure, and also did not include an oxide shell (including 30 Wt% Al$_2$O$_3$ gives 3625 K for the adiabatic reaction temperature, only a slight difference). The list of gaseous species is certainly incomplete, and we have only listed the major gas species predicted to occur during the thermite reaction. There are several other minor gases that are predicted to form, including but not limited to Al, Al$_2$O, AlO, AgI, and Cu$_2$. Also, there are also some species that may not be contained in the thermodynamic database used by the CEA software, and so the adiabatic flame temperature listed for Al/AgIO$_3$ should be considered as an approximate value. With these points in mind, we can see in Table 1 that the Al/AgIO$_3$ thermite has a higher adiabatic flame temperature and also has the potential to produce more gas than the two metal oxide thermites. It can be seen in the case of the metal oxides that the adiabatic reaction temperature is limited by the metal boiling points, whereas for the AgIO$_3$, the adiabatic reaction temperature is limited by dissociation of Al$_2$O$_3$. The high adiabatic flame temperature, along with the gas release capabilities, indicate that AgIO$_3$ should perform very well in burning tests, and this is experimentally verified.

EXPERIMENTAL

Sample Preparation

The nanoaluminum samples used in this work were purchased from the Argonide Corporation (designated as "50 nm ALEX") and from NanoTechnologies (80 nm size). TGA showed the aluminum to be 70% (ALEX Al) and 72% (80 nm Al) elemental by mass, and only this portion is considered when determining the equivalence ratio. The CuO and Fe$_2$O$_3$ (<100 nm as specified by the supplier) used

in the pressure cell and wire studies were purchased from Sigma Aldrich, and a second CuO sample (45 nm average particle size as determined by surface area analysis) was provided by Technanogy. Micron-sized silver iodate was purchased from City Chemical, and had a specific surface area of $0.9 \, m^2/g$, corresponding to a particle size of $1.2 \, \mu m$, based on uniform spherical particles. A larger sized (5–400 μm) silver iodate, obtained from Baker & Adamson, was sieved (−60 mesh) and ball-milled to reduce the size to 900 nm, based on specific surface area (this sample was only used in thermal analysis experiments). Nanoscale silver iodate was prepared by precipitation from aqueous solutions of silver nitrate and potassium iodate or sodium iodate, using a modification of a literature method (Sendroy, 1937). A solution of 30.97 g of $AgNO_3$ in 125 mL of water was added over 45 s to a solution of 39.58 g of KIO_3 (1.4% molar excess) in 950 mL of water, with rapid mechanical stirring. The resulting mixture was stirred for 5 min, then filtered and washed with water, water/acetone mixture, acetone, and ether. After air drying on the fritted funnel, the product was further dried in an oven at 403 K for 10 hr. Surface area analysis by nitrogen adsorption gave a specific surface area of $6.95 \, m^2/g$, which would correspond to a particle size of 156 nm for uniform spherical particles. A similar preparation using sodium iodate reagent produced a powder with a specific surface area of $4.0 \, m^2/g$, corresponding to a spherical particle size of 270 nm. However, the actual particle morphology consists of thin platelets, roughly 1 μm in diameter. Silver iodide was purchased from Sigma Aldrich, and the size was not specified by the supplier.

Thermite samples were prepared by weighing the aluminum and oxidizer components (stoichiometric), then adding ∼10 mL of hexane. The samples were then ultrasonicated in a sonic bath for 30 min to ensure intimate mixing. For the wire tests, a micropipette was used to coat the wire with the hexane/thermite mixture, and the hexane allowed to evaporate. For the pressure cell tests, the hexane/thermite mixture was first evaporated at room temperature and finally at 373 K for a few minutes to drive off any remaining hexane. The dry powder was then gently broken up with a spatula to remove any large clumps, and until the consistency was that of a loose powder.

We must note that the degree of mixing achieved in each sample was not studied in this work. A scanning electron micrograph of an $Al/AgIO_3$ nanocomposite powder is presented in a reference (Johnson et al., 2008), and shows that mixing is limited by clumping of both ingredients. The $AgIO_3$ has a platelet-like morphology, and could potentially mix differently than spherical nanoparticles under the same amount of ultrasonication. Ideally, all of the oxidizers studied would have exactly the same morphology so that there was no difference in the homogeneity or mixing of the materials, but this was not the case. We chose a 30-min sonication time primarily from past experience that this amount of time gave the best reproducible conditions. If the time is too short, the mixing is poor and batch-to-batch variations occur, whereas too long of a sonication time caused some material to stick to the vial walls.

Fast-Heated Wire Tests

Measuring the ignition temperature in nanocomposite materials is complicated by the fact that the ignition mechanism is likely dependent on the heating rate. It is

not uncommon for the reported ignition temperature to be several hundred degrees different depending on what experimental technique was used to heat the particles. As discussed in a review article by Dreizin (2009), an appropriate experiment would be one that heats the sample uniformly and with high heating rates.

In a recently developed temperature-jump/time-of-flight mass spectrometer (T-Jump/TOFMS) system (Zhou et al., 2009), we coated a thin platinum wire (76 μm diameter) with a very small amount of sample (<0.03 mg). The wire is then rapidly joule heated using a tunable voltage pulse to achieve heating rates up to $\sim 5 \times 10^5$ K/s and a maximum temperature of ~1800 K. By simultaneously monitoring the transient resistivity of the wire, the temporal temperature distribution can be calculated. To investigate the decomposition and combustion processes, the coated platinum wire is inserted into the high vacuum region of the mass spectrometer close to the ionization region. The wire is rapidly heated and the gaseous product species are ionized using an electron gun. Sampling of the product species by the mass spectrometer occurs simultaneously to the sample heating so that time resolved mass spectra can be obtained at a rate of 10,000 Hz. The TOFMS system was originally designed to determine elemental composition in a single particle (Lee et al., 2003), and thus is highly sensitive to the mass (~femtograms). A more detailed description of the modified experimental setup is given elsewhere (Zhou et al., 2009).

To determine the ignition temperature, the wire is heated in air at atmospheric pressure and the optical emission is monitored by a photomultiplier tube. Ignition is said to have occurred when the optical signal reaches 2% of its maximum value. Three shots are performed for each sample, and the average value is taken to be the ignition temperature. The uncertainty in the ignition temperature is estimated to be 40 K, based on several factors, including the length of the wire, and contact resistance.

Pressure Cell Combustion Tests

A fixed mass (25 mg) of the loose thermite powder is placed in a constant-volume pressure cell (Prakash et al., 2005; Sullivan et al., 2007; Sullivan and Zachariah, 2009) and ignited by resistive heating of a nichrome wire. A piezoelectric pressure transducer is attached to one port of the cell, while a lens tube assembly is attached to the other to collect the light and focus it onto a photodiode. The transient optical and pressure signals are captured simultaneously using a digital oscilloscope. The pressurization rate is calculated by dividing the maximum pressure by the rise time of the pressure signal, and is reported as a relative measurement of the reactivity. The pressurization rate has been used to report reactivity since it has been shown to correlate with flame propagation velocities (Son et al., 2002), another commonly used measurement of reactivity. The burn time of the thermite is taken to be the full width at half-maximum (FWHM) of the optical signal.

We must stress that both the pressurization rate and luminosity measurements should only be thought of in terms of relative performance at the present time. As mentioned, the pressurization rate has been shown to experimentally correlate with flame propagation rates, and thus is considered to be somehow proportional to the reaction rate. We recently argued that the luminosity could be used as a measurement of burning time, but this assumption was only based on experiments that

showed the optical signal to be independent of the sample mass, and also because optical emission has long been used to measure particle burning times. Until some controlled experiments can be carried out on materials with well-defined characteristics, both of these measurements should be treated with some skepticism for now and are only used to show relative comparisons between the $AgIO_3$ system and other more common thermites.

Thermal Analysis, Surface Area Analysis, and High-Speed Video

Simultaneous differential scanning calorimetry and thermogravimetric analysis (DSC-TGA) was conducted on a TA Instruments Q600 SDT. The $AgIO_3$ sample was the ball-milled Baker & Adamson material (900 nm). A 4.28 mg sample was heated from room temperature to 1073 K at 5 K/min under a flow of nitrogen gas. A second experiment was conducted at a higher heating rate, 50 K/min, using a 5.72 mg sample. This sample was also held at 1073 K for 30 min. Surface area analysis was conducted on a Quantachrome Autosorb 1C surface analyzer, using low-temperature nitrogen adsorption. High-speed digital video imaging was conducted with a Vision Research Phantom v9.1 camera.

Postreaction Analysis

The reacted product was collected after combustion in the pressure cell by scraping the product off of the sample holder and into a ceramic crucible with some hexane. The crucible was sonicated for several minutes, and a pipette was used to dropper the sample onto a grid (Au mesh/Carbon film) for analysis in a high-resolution transmission electron microscope (TEM, JEOL JEM 2100 FEG). The TEM is equipped with an energy dispersive X-ray spectrometer (EDS, Oxford INCA 250), which can be operated in scanning mode to perform 1D elemental line scans and 2D elemental maps of the sample. The dry powdered product was collected and prepared for X-ray diffraction (XRD, Bruker C2 Discover with GADDS, operating at 40 kV and 40 mA with unfiltered Cu Kα radiation, $\lambda = 1.5406\,\text{Å}$) analysis to determine any crystal structures that may form during the reaction.

Thermodynamic Properties

Thermodynamic data involving reactions of $AgIO_3$ and AgI were obtained from the database of the Facility for the Analysis of Chemical Thermodynamics (http://www.crct.polymtl.ca/reacweb.htm). The database is supported by the Center for Research in Computational Thermochemistry at École Polytechnique in Montreal, Canada.

RESULTS AND DISCUSSION

The experimental results presented in this work were conducted at both the University of Maryland and at China Lake. The results were combined in this paper, and for that reason, different materials and mixing parameters have been used depending on the experiment. A table summarizing all of the experiments, along with

Table 2 A table of all experiments carried out, along with the equivalence ratio and particle sizes/sources

Experiment	Sample studied	Equivalence ratio	Fuel, size	Oxidizer, size
Fast heated	Al/Fe$_2$O$_3$	1.0	ALEX, 50 nm	Sigma-Aldrich, <100 nm
wire	Al/CuO	1.0	ALEX, 50 nm	Sigma-Aldrich, <50 nm
	Al/AgIO$_3$	1.0	ALEX, 50 nm	Synthesized, 156 nm
	AgIO$_3$	N/A	N/A	Synthesized, 156 nm
	AgI	N/A	N/A	Sigma-Aldrich, not given
Simultaneous	AgIO$_3$	N/A	N/A	Baker & Adamson
TGA/DSC	(Fig. 1)			Ball-Milled, ~900 nm
Powder burn	Al/AgIO$_3$	1.12	NanoTech, 80 nm	Synthesized, 270 nm
(Fig. 4)	Al/AgIO$_3$	1.06	NanoTech, 80 nm	City Chemical, 1200 nm
	Al/CuO	1.27	NanoTech, 80 nm	Technanogy, 45 nm
Pressure cell	Al/Fe$_2$O$_3$	1.0	ALEX, 50 nm	Sigma-Aldrich, <100 nm
	Al/CuO	1.0	ALEX, 50 nm	Sigma-Aldrich, <50 nm
	Al/AgIO$_3$	1.0	ALEX, 50 nm	Synthesized, 156 nm
XRD/TEM/	Al/AgIO$_3$	1.0	ALEX, 50 nm	Synthesized, 156 nm
EDS	(From Cell Figs. 5–7)			
SEM/EDS	Al/AgIO$_3$	1.25	NanoTech, 80 m	Synthesized, 181 nm
	(From Plate Fig. 8)			

the materials and equivalence ratios used, is shown in Table 2. We expect only subtle differences between using different aluminum and CuO suppliers, and the slight variance in equivalence ratio was done in order to compare the maximum performance in the open powder burning experiments. As previously discussed, the pressurization rate is a relative measurement, so the equivalence ratio was kept constant to make a direct comparison between systems. Optimizing the equivalence ratio for each oxidizer would have altered the values slightly, but the generalized trend would still exist.

Combustion Characterization

The ignition temperature of stoichiometric Al/AgIO$_3$ in air and at atmospheric pressure measured using the hot wire setup at a heating rate of 5×10^5 K/s was found to be 1215 ± 40 K. In comparison and for the sake of discussion, the ignition temperatures of Al/CuO and Al/Fe$_2$O$_3$ under the same conditions are 1220 ± 40 K and 1510 ± 40 K, respectively. For both CuO and Fe$_2$O$_3$ (Sigma Aldrich), we have studied the oxidizer thermal decomposition using the T-Jump/TOFMS with and without the aluminum fuel. The results show that O$_2$ release occurs prior to evidence of reaction (Al, Cu, Fe species), indicating that the thermite ignition mechanism involves some degree of thermal decomposition of the oxidizer to a suboxide and O$_2$ gas.

Constant temperature and pressure (TP) equilibrium calculations using NASA's CEA software show that CuO decomposes to Cu$_2$O and O$_2$, and Fe$_2$O$_3$ decomposes to Fe$_3$O$_4$ and O$_2$ under atmospheric conditions at approximately 1400 K and 1700 K, respectively. It should be noted that the decomposition can start occurring at lower temperatures, but at the reported values a large increase in the

decomposition was seen to occur in the NASA CEA calculations. It should also be noted, and is shown later, that the decomposition mechanism may change at high heating rates, so the decomposition temperatures are only listed for the sake of discussion. These calculated temperatures are consistent with the experimental ignition temperatures within $\sim$200 K, and the difference could easily be attributed to the wide range of particle sizes and thus melting/decomposition temperatures within the sample, or to inaccuracies in the calculation. Combining the experimental results with the thermodynamic calculations, it is reasonable to speculate that the ignition of Al requires a critical partial pressure of O_2 to be reached in order to overcome heat losses and facilitate the ignition of the fuel.

Stern (2001) indicated that under atmospheric conditions, $AgIO_3$ decomposes to AgI and O_2 around 678 K and includes a few references supporting this. We investigated the thermal behavior of $AgIO_3$ in more detail by both slow- (DSC-TGA) and fast-heating (hot wire mass spectrometry) experiments. Figure 1 shows DSC-TGA analysis of the 900 nm $AgIO_3$. Three endotherms are observed in the temperature range of 670–840 K, attributed to melting of $AgIO_3$ near 692 K, followed by decomposition to AgI around 740 K, and melting of AgI at 827 K. The sample exhibited an 18% weight loss during the second endotherm, consistent with the 17% calculated weight loss for conversion of $AgIO_3$ to AgI. Visually, heating of $AgIO_3$ in air resulted in melting, followed by gas evolution and a color change from colorless to a yellow liquid (AgI is yellow). The third endotherm temperature matches the literature value for the melting point of AgI (831 K; Lide, 1998). Further heating of the sample above the melting point of AgI resulted in an increased rate of weight loss until the experiment ended by reaching 1073 K (where the total weight loss was
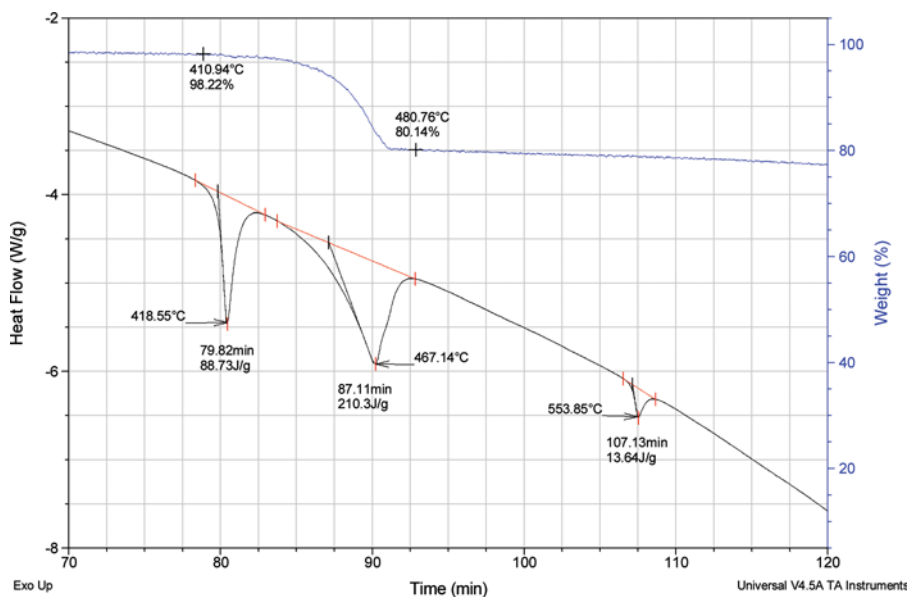
Figure 1 Thermal analysis by DSC-TGA of $AgIO_3$ heated under nitrogen at 5 K/min. The $AgIO_3$ was commercial micron sized $AgIO_3$ ball milled down to a particle size of around 900 nm.

66%). This higher temperature weight loss appears to be due to evaporation of the AgI product (b.p. 1779 K; Lide, 1998). Holding the sample at 1073 K for 30 min resulted in a total weight loss of 84%, confirming that both Ag and I are lost from the sample at this temperature. Integration of the endotherms gives approximate enthalpies for fusion of AgIO$_3$ (25 kJ/mol), decomposition to AgI (60 kJ/mol), and fusion of AgI (4 kJ/mol). The literature value for the heat of fusion of AgI is considerably higher at 9.4 kJ/mol (Lide, 1998), indicating that some of the AgI was probably in liquid form prior to the endotherm. The calculated enthalpy of decomposition of solid AgIO$_3$ to solid AgI, 116 kJ/mol, is similar to the observed total of 85 kJ/mol for fusion and decomposition of AgIO$_3$. In a second DSC-TGA experiment conducted at 50 K/min the three minima for the endotherms shifted to 706 K, 807 K, and 833 K. The endotherm for the AgIO$_3$ decomposition had by far the largest shift to higher temperature, about 67 K, for the tenfold increase in heating rate.

Thermal decomposition of the 156 nm AgIO$_3$ at high heating rates was investigated by conducting the hot wire experiment using the T-Jump/TOFMS. From the experimental results, we detect the release of O$_2$, O and I, above 1150 K, which is about 350–400 K higher than the temperature observed in the DSC-TGA experiments. The release profile is plotted along with the wire temperature in Figure 2. We do not detect any silver or silver iodide (AgI) gas formation. These results indicate that at high heating rates, the decomposition mechanism has completely changed from what was observed in the DSC-TGA experiment. A possible mechanism involving the release of iodine and oxygen could involve the formation of the known compound Ag$_5$IO$_6$, analogous to the decomposition of Ba(IO$_3$)$_2$, which forms Ba$_5$(IO$_6$)$_2$ (Wiberg and Holleman, 2001). Iodine has also been reported in the thermal decomposition of NaIO$_3$, where about 28% of the salt decomposes to Na$_2$O, I$_2$, and O$_2$, with the rest decomposing to NaI and O$_2$ (Erdey et al., 1968).
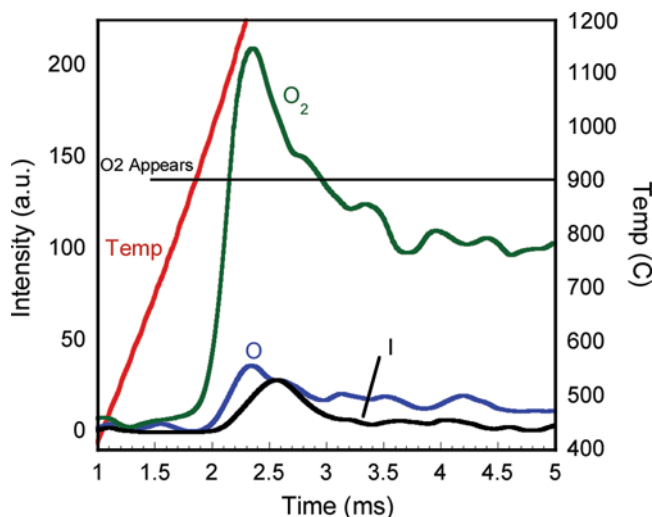
Figure 2 Transient gas release profile as determined by rapidly heating AgIO$_3$ in the mass spectrometer. The material is the synthesized 156 nm AgIO$_3$.

In order to further examine the decomposition mechanism, AgI was also tested on the wire. In this case we see a small AgI signal with a relatively large Ag and I signal occurring concurrently. This sort of behavior is consistent with the AgI being evaporated and then being cracked by the electron beam into elemental Ag and I, otherwise we would expect to see the emergence of Ag and I at different temperatures corresponding to their individual vaporization temperatures. In any case, the AgI results showed a very different spectrum than the $AgIO_3$. The results imply that AgI is not an intermediate product in the decomposition of $AgIO_3$ at high heating rates, and would therefore suggest that the decomposition mechanism is more likely analogous to that observed for $Ba(IO_3)_2$. It also suggests that thermal analysis techniques may not necessarily be accurate in predicting decomposition behavior under very intense heating rates.

The experimental ignition temperature of $Al/AgIO_3$ (1215 K) is well above the point where $AgIO_3$ is found to decompose and release oxygen using slow heating thermal analysis ($\sim$740 K). However, it does correlate with the O_2 release temperature experimentally seen in the mass spectrometer (1173 K) at high heating rates. Although the decomposition mechanism is evidently different at high heating rates, we see experimentally that the release of O_2 is an important part of the ignition mechanism, consistent with CuO and Fe_2O_3. Analogous to these systems, we may speculate that the ignition in the $Al/AgIO_3$ thermite may be dependent on the thermal decomposition of $AgIO_3$ to provide a critical partial pressure of O_2 to ignite the aluminum.

Next we record a video of the thermite sample heated on the wire in vacuum and at atmospheric conditions. At atmospheric conditions, we see a violent reaction and evidence of the unreacted powder being lifted off the wire. A series of snapshots of the powder burning on the wire is shown in Figure 3. What can be seen is that the unreacted powder can be propelled away from the wire prior to any luminescence or burning. Nanoparticles have very fast characteristic flow relaxation times, meaning that they can easily be picked up and swept forward by gas. If the oxidizer is thermally decomposing to release O_2 or other gases such as iodine, the hot decomposition gases could be responsible for a large part of the convective heat transfer, while also propelling the unreacted powder forward. This behavior could lead to propagation rates that occur much faster than the characteristic burning time of the fuel particles.

In the mass spectrometer (10^{-7} torr), the thermite showed visual signs of burning but it was clearly less violent than at atmospheric conditions. We also collected the time-resolved mass spectra, and found the data to be similar to the pure $AgIO_3$ (O_2, I, and O release), but the rise times of these signals were faster. The heat liberated during the reaction seems only to be further decomposing the oxidizer. Although the $Al/AgIO_3$ thermite does show visual signs of reacting under vacuum, it is important to be careful about interpreting the results. The mean free path of gas molecules under a vacuum is orders of magnitude higher than in air, and so some oxygen may simply escape from the thermite before it reacts with the aluminum. Also, the interparticle heat transfer may be hindered due to the lack of interstitial air to rapidly conduct or convect heat to adjacent particles. Therefore, it's possible that the temperature does not reach the adiabatic flame temperature, and thus species such as Ag vapor may not be seen in this system, but may exist for larger samples reacted at atmospheric pressures.
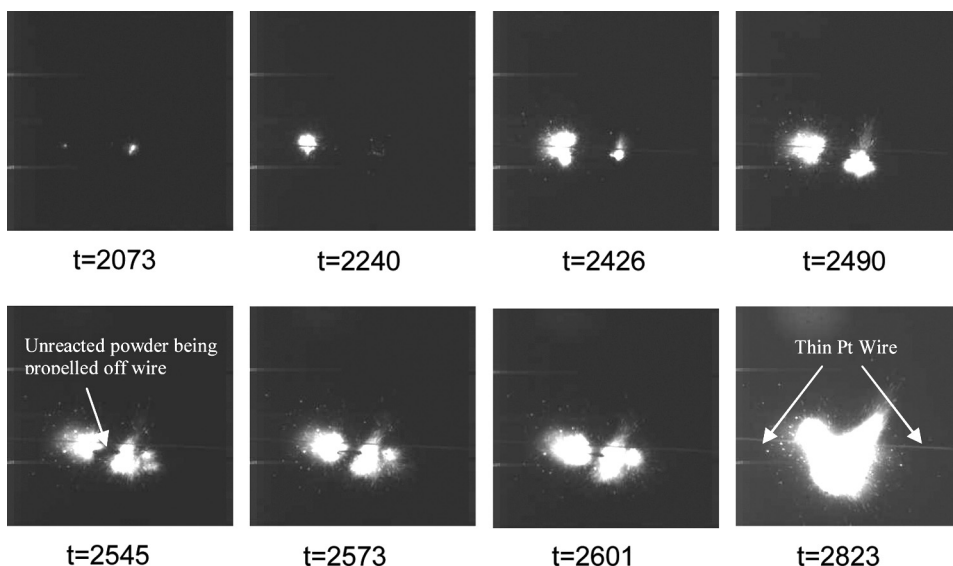
Figure 3 Sequential snapshots of Al/AgIO$_3$ burning in air. The wire can only faintly be seen, and remains stationary throughout the burning. The thermite is Al (ALEX) and AgIO$_3$ (156 nm), with an equivalence ratio of 1.0.

Combustion cell tests were used to evaluate Al/AgIO$_3$ relative performance against other thermites under atmospheric conditions. The experimentally measured pressure and optical data is tabulated for Al/AgIO$_3$ along with a relatively slow (Al/Fe$_2$O$_3$) and fast (Al/CuO) thermite for comparison in Table 3. Clearly the Al/AgIO$_3$ system significantly outperforms both other oxidizers in terms of relative performance, achieving a much higher peak pressure and pressurization rate. Combining the mass spectrometer results with the thermodynamic predictions, the improved performance is likely a combination of higher reaction temperatures and enhanced gas release during the oxidizer decomposition.

We recently argued that the initial pressure spike for a fast-burning MIC (i.e., Al/CuO) is mainly attributed to the oxidizer decomposition because the decomposition happens at a temperature well below the adiabatic flame temperature (Sullivan and Zachariah, 2009). As the aluminum is ignited and begins to burn, we argued that the energy liberated by the reaction further causes the oxidizer to thermally decompose and release gas, thus pressurizing the system, followed by the remainder of the

Table 3 Pressure cell data for Al/AgIO$_3$ along with a relatively slow (Al/Fe$_2$O$_3$) and fast (Al/CuO) thermite (CuO and Fe$_2$O$_3$ from Sigma-Aldrich)

	Al/Fe$_2$O$_3$	Al/CuO	Al/AgIO$_3$
Pressure rise (psi)	13.4	116	296
Pressure rise time (μs)	800	13	5.3
Pressurization rate (psi/μs)	0.017	9.0	57
FWHM burn time (μs)	936	192	172

aluminum burning. In the pressure cell tests, this is experimentally seen as a fast pressure spike followed by an optical emission signal over a much longer timescale. We proposed that the burning mechanism in such a system is similar to the burning of aluminum in a pressurized, oxygenated environment. For the $Al/AgIO_3$ thermite, we see the same characteristic behavior; a fast initial pressure spike followed by a longer optical burning time.

In comparing the pressure cell data for Al/CuO and $Al/AgIO_3$ (Table 3), it is seen that both thermites have approximately the same burning time but very different pressurization behavior. If both systems were thermally decomposing and releasing oxygen, followed by the remainder of the aluminum burning, then we would expect similar times because the burning would be rate-limited by the aluminum in both cases. The large difference in pressurization is likely attributed to the decomposition products of the two oxidizers. $AgIO_3$ can release significantly more gas upon thermal decomposition (i.e., O_2, O, and I). If the temperature was able to quickly approach the adiabatic flame temperature listed in Table 1, some amount of Ag could also be vaporized and thus contribute to the pressure.

Combustion tests were also conducted on loose powder samples placed along a line on a supporting aluminum pan. Propagation rates were determined by high-speed video imaging, with the results presented in Figure 4. Combustion proceeded steadily across the samples, giving propagation rates of 630 m/s for a sample
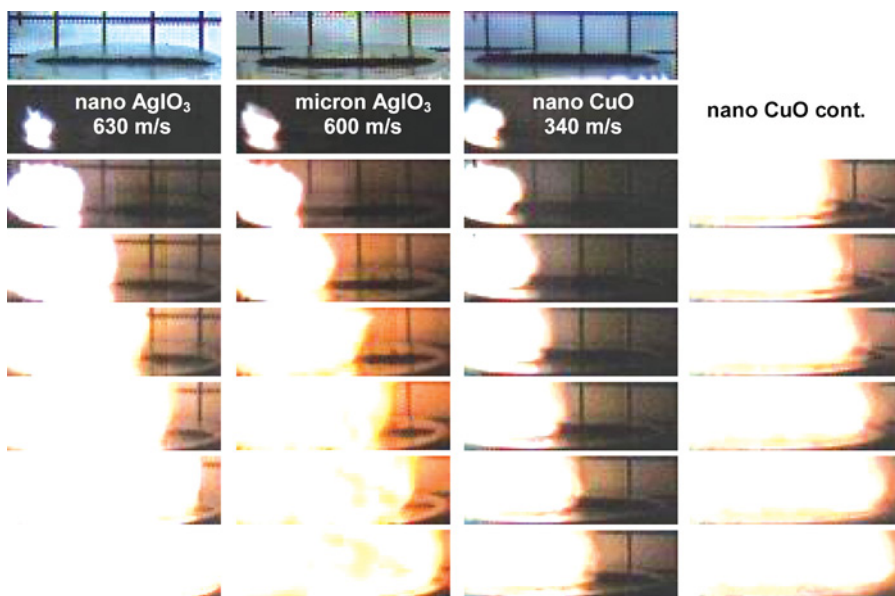
Figure 4 Video images of the combustion of three thermite samples in air. The images at the top show the samples prior to combustion, with a 45-mg line of powder placed on an aluminum support. A grid directly behind the sample has a spacing of 10.8 mm between lines. Samples were ignited by a spark from a wire attached to a tesla coil (tip of wire visible in the upper left corner of the top images). Images were recorded at 10-μs intervals, using a 2-μs exposure. The Al in this study is 80 nm from NanoTechnologies. The CuO in this study is 45 nm from Technanogy. Each sample was fuel rich in this study with equivalency ratios of 1.12 for the nano $AgIO_3$ material, 1.06 for the micron $AgIO_3$ material, and 1.27 for the CuO material.

composed of 80 nm Al/270 nm AgIO$_3$, 600 m/s for 80 nm Al/1.2 μm AgIO$_3$, and 340 m/s for 80 nm Al/45 nm CuO (Technanogy). The propagation rate for Al/CuO (where the equivalence ratio was 1.27) is similar to the ~500 m/s reported in an open tray burn test (Sanders et al., 2007). As with the combustion cell tests, the AgIO$_3$ oxidizer gave a higher reactivity compared to CuO. Surprisingly, the micron-sized AgIO$_3$ thermite had nearly the same propagation rate as the nanothermite. If the characteristic heating and decomposition times of the oxidizer are much faster than the characteristic reaction time of the aluminum, then this behavior may be expected. However, further work would be required to verify this. The combustion tests and the measured high propagation rate of the micron AgIO$_3$ thermite are consistent with a mechanism in which the AgIO$_3$ rapidly decomposes and releases iodine and also oxygen, which then reacts with Al.

Post-combustion Characterization

In biocidal applications, the nature and dispersion of the product may supersede the importance of the actual combustion performance. A representative TEM image along with the elemental maps of Al, O, I, and Ag is shown in Figure 5 for products from the pressure cell test. Unfortunately, the image quality was limited by instability of the material under the electron beam, where prolonged exposure induced morphological changes. This behavior is somewhat common when trying to image species such as iodine, which can readily ionize or vaporize under an intense
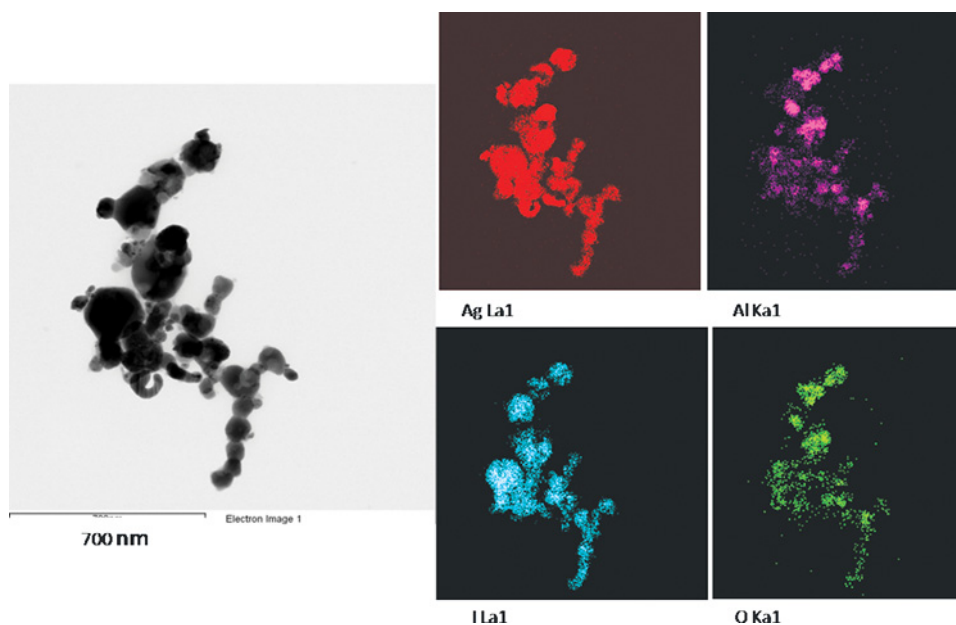
Figure 5 Representative TEM image and 2D elemental maps (using EDS) of Ag, Al, I, and O after reaction inside the combustion cell. Higher resolution images could not be achieved due to beam interactions and morphological changes in the sample with prolonged beam exposure. The thermite was Al (ALEX) and synthesized AgIO$_3$ (156 nm) with an equivalence ratio of 1.0.

electron beam. We see particles that contain Al and O, and other particles which contain both Ag and I. In several cases, we see particles that appear to contain all four elements. Two such particles are shown in Figure 6 along with an elemental line-scan coupled with elemental analysis. The results show the formation of a core-shell structure of Al_2O_3 surrounded by Ag and I. In the next section we confirm via X-ray diffraction that this is actually AgI. Conceptually, this core shell structure could form since Al_2O_3 has a relatively high boiling/decomposition point ($\sim$4000 K). Either the Al_2O_3 never exists in the gas phase, or upon cooling, will be the first species to condense. The Ag and I then somehow recombine, either through gas phase recombination reactions or heterogeneous surface reactions, and coat the Al_2O_3 surface before solidifying. The actual mechanism or extent of coating is beyond the scope of the work, but it is important to mention that we do see that the biocidal agent is exposed to the environment post-reaction, and is not trapped (i.e., as the core in core-shell structure).

Figure 7 shows XRD patterns for pure $AgIO_3$, along with unreacted and reacted $Al/AgIO_3$ thermites. What we see is the disappearance of Al and $AgIO_3$ spectra and the emergence of AgI in the product. Most of the peaks in the XRD pattern match well with γ-AgI, which is the dominant polymorph obtained when AgI is rapidly cooled from its melting point (Burley, 1963). The presence of a lesser amount of the β polymorph of AgI is indicated by the peak near $2\theta = 22$. The alumina that forms exhibits only weak peaks in the XRD pattern. The peak at $2\theta = 67$, along with the shoulder at 45.5°, are likely due to δ-Al_2O_3, which is commonly observed when molten Al_2O_3 rapidly crystallizes, such as in the synthesis of nanophase alumina by arc plasma (Kumar et al., 1999). Elemental silver was not detected by XRD, so it appears that the biocidal reaction product of $Al/AgIO_3$ is almost entirely AgI.
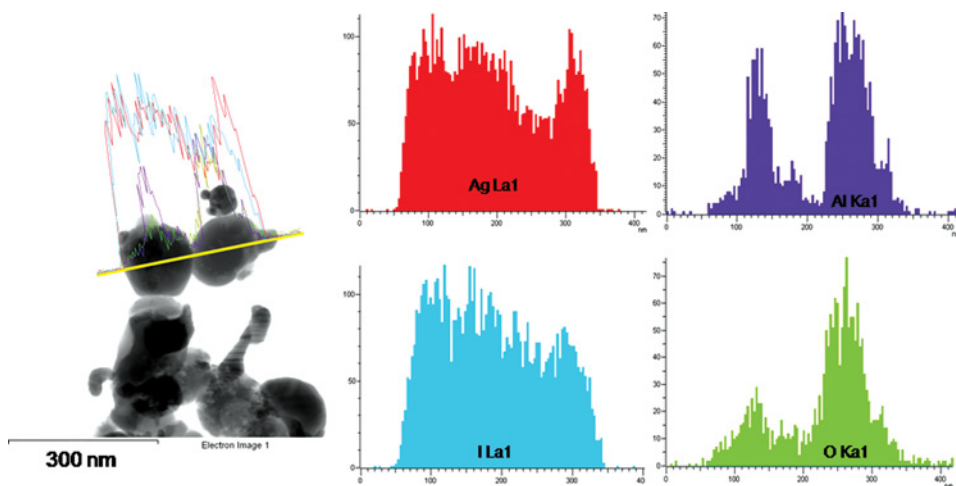
Figure 6 TEM image and 1D elemental linescan (using EDS) across two adjacent particles of $Al/AgIO_3$ reacted in the pressure cell. Note the presence of an Al/O core surrounded by AgI in each particle. The extra (green) line shown in the image was carbon from the film. The thermite was Al (ALEX) and synthesized $AgIO_3$ (156 nm) with an equivalence ratio of 1.0.
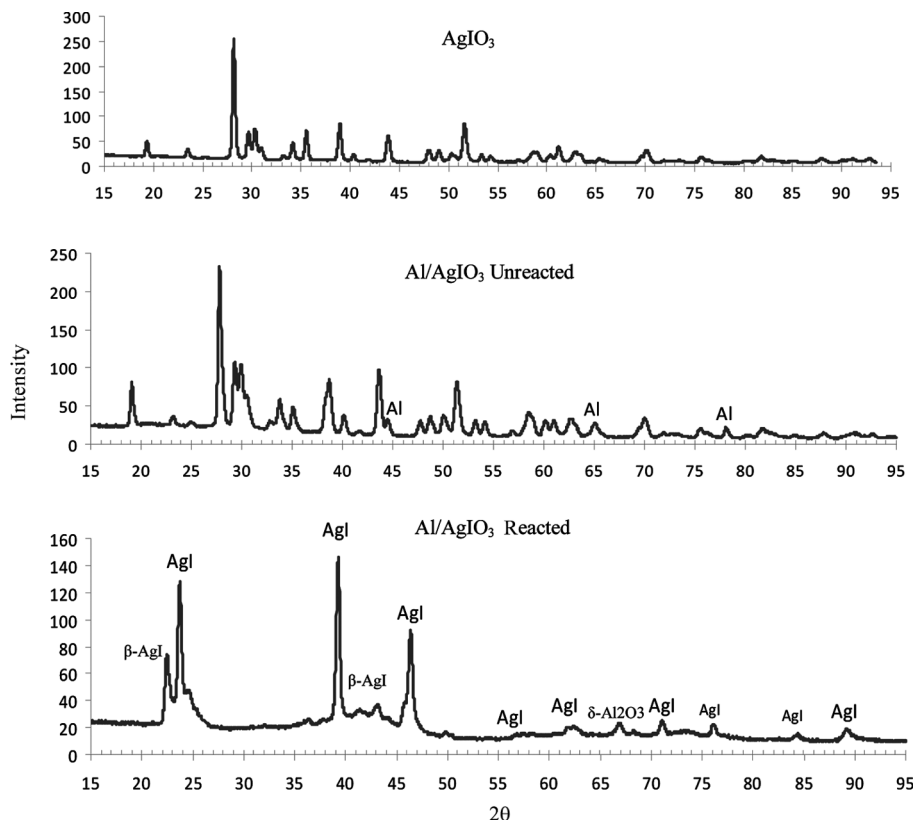
Figure 7 XRD patterns (Intensity vs. 2θ) for pure AgIO$_3$, along with the thermite before and after reaction in the pressure cell. The major detectable reaction product is AgI. Unless otherwise noted, the AgI peaks are γ-AgI. The thermite was Al (ALEX) and synthesized AgIO$_3$ (156 nm) with an equivalence ratio of 1.0.

Segregated AgI and aluminum oxide products have also been identified in an experiment conducted to quench the hot products from the thermite reaction. A 20 mg sample was placed at the center of one copper plate, and a second plate was placed parallel to and 10 mm above the first plate. The sample was initiated with a spark. Residue collected on the top plate at a point directly above the original sample consists mainly of micron-scale globular structures, as shown in micrographs a, b, and d in Figure 8. This deposit is highly enriched in Al (and O), based on the overall atomic ratio of 10 Al per Ag in this region, versus a ratio of 2.5 in the thermite. Elemental mapping indicates that all of the micron-scale features are predominantly aluminum oxide. Spot EDS analysis shows that some of the submicron particles are highly enriched in Ag (Ag:I ratio approximately 5:1), as marked in micrograph d. Overall, the Ag:I ratio was 4:3 in this region, and an elemental map of iodine showed essentially uniform occurrence, except in the area of the large aluminum oxide particle in the upper left corner of micrograph b. This large smooth particle may have cooled slower than the smaller aluminum oxide deposits, resulting in less condensation of AgI on the surface. Residue from a region 10 mm away from
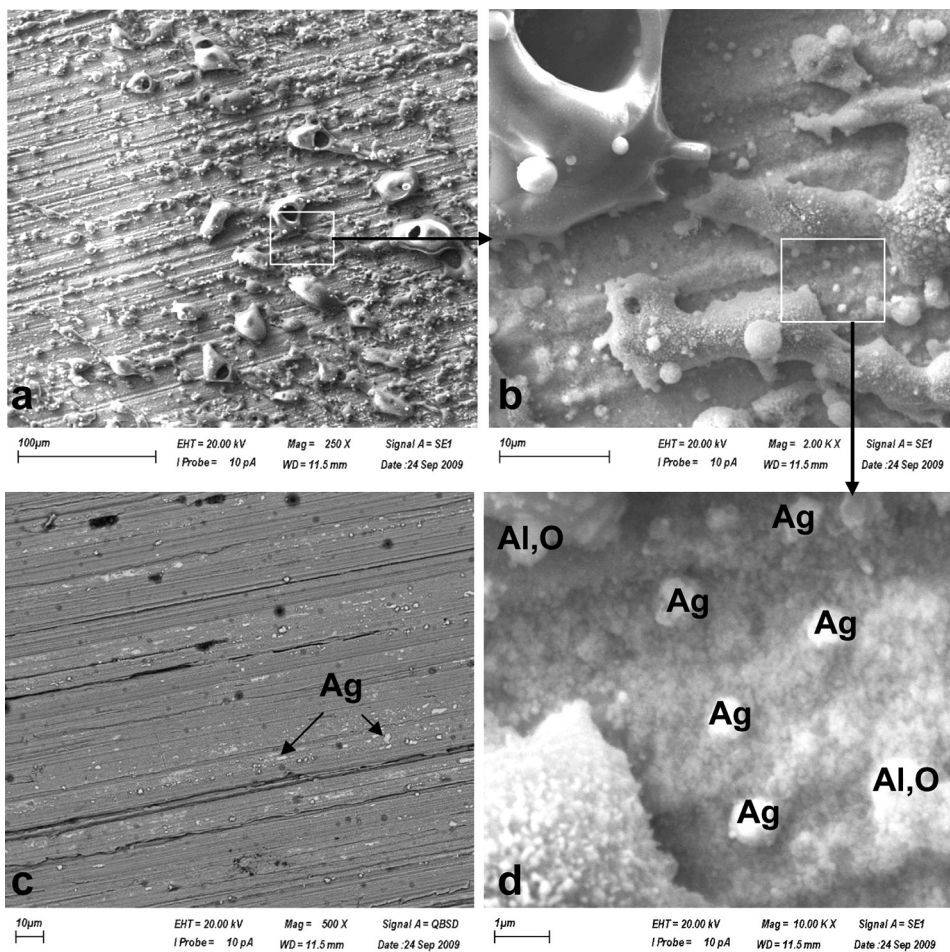
Figure 8 Scanning electron micrographs of reaction products from spark initiated nano $Al/AgIO_3$ (20 mg) deposited on a copper plate. Micrographs a, b, and d (taken at different magnifications) show the region of the copper plate that was positioned 10 mm directly above the sample. Micrograph c shows a region of the copper plate that was 10 mm distant from the spot of the top micrograph. Micrograph c was taken in the quantum backscatter mode, where the light elements (Al, O) appear as dark spots in the image, while the heavy elements (Ag, I) appear as light spots. Small islands of elemental Ag (essentially free of iodine) are marked in micrograph c. The nearly horizontal lines result from abrasive polishing of the copper plate. The Al was from Nanotechnologies, and the $AgIO_3$ was synthesized (181 nm).

the center of the top plate is shown in the micrograph in Figure 8c. This area contains rather sparse deposits identified mainly as micron-sized aluminum oxide spherical particles, ≤ 100 nanometer AgI particles, and some micron-sized islands of elemental Ag. In this region the Al/Ag ratio is 1.6. The center region would be the hottest region during the reaction, where molten aluminum oxide deposited (m.p. 2327 K). This region is depleted of Ag and I, probably by transport of the vapor to cooler regions. Both regions analyzed contain nearly stoichiometric Ag and I, consistent with the observation of AgI as the predominant Ag product by

XRD analysis. However, small amounts of elemental silver deposits were also observed, including nanoparticulates.

From the postreaction analysis, we do see that high surface area nanoparticles of the biocidal elements are formed. Furthermore, both Ag and I are surface exposed (i.e., not trapped within the interior of a particle).

CONCLUSION

AgIO$_3$ was investigated as an oxidizer in nanoaluminum-based thermites, in particular for systems designed for biocidal activity. The ignition temperature of the Al/AgIO$_3$ was determined to be 1215 ± 40 K for rapid heating on a wire. Mass spectrometry showed that the AgIO$_3$ decomposed into O$_2$, O, and I. High-speed imaging showed that the reaction proceeded violently in air, with ejection of powder radially away from the wire. Pressure cell tests showed that the Al/AgIO$_3$ significantly outperformed Al/CuO in pressurization rate, although both systems show nearly the same burning time. This suggests that the burning mechanisms are similar and rate-limited by the aluminum. The pressurization enhancement is likely attributed to the enhanced gas release as AgIO$_3$ decomposes, along with the higher energy content and reaction temperature of this system. Postreaction analysis was performed, and XRD showed primarily AgI as the crystalline reaction product. Electron microscopy with elemental analysis indicated that the silver iodide products were generally spherical and agglomerated, with the AgI covering some of the surfaces of aluminum oxide to form core-shell particles.

ACKNOWLEDGMENTS

REFERENCES

Burley, G. 1963. Polymorphism of silver iodide. *Am. Mineral*, **48**, 1266.

Dreizin, E.L. 2009. Metal-based reactive nanomaterials. *Progress in Energy and Combustion Science*, **35**, 141.

Erdey, L., Simon, J., and Gal, S. 1968. Thermoanalytical properties of analytical grade reagents vs. sodium halates. *Talanta*, **15**, 653.

Fischer, S.H., and Grubelich, M.C. 1998. Theoretical energy release of thermites, intermetallics, and combustible metals. *24th International Pyrotechnics Seminar*, Monterey, CA.

Johnson, C.E., Higa, K.T., and Albro, W.R. 2008. Nanothermites with condensable gas products. *Proceedings of the International Pyrotechnics Seminar*.

Klein, P.M.G., and Woodhouse, J. 2006. U.S. Patent No. 7,033,509. U.S. Patent and Trademark Office, Washington, DC.

Kumar, P.M., Balasubramanian, C., Sali, N.D., Bhoraskar, S.V., Rohatgi, V.K., and Badrinarayanan, S. 1999. Nanophase alumina synthesis in thermal arc plasma and characterization: Correlation to gas-phase studies. *Materials Science and Engineering B*, **B63**, 215.

Lee, D., Sakurai, H., Mehadavan, R., and Zachariah, M.R. 2003. Measurement of condensed-phase reaction kinetics in nanoparticles using single particle mass spectrometry. *Abstracts of Papers of the American Chemical Society*, **225**, 520.

Lide, D.R. (Ed.). 1998. *CRC Handbook of Chemistry and Physics*, CRC Press, New York.

Merck. 2001. *The Merck Index*, Author, Whitehouse Station, NJ.

Morones, J.R., Elechiguerra, J.L., Camacho, A., Holt, K., Kouri, J.B., Ramirez, J.T., and Yacaman, M.J. 2005. The bactericidal effect of silver nanoparticles. *Nanotechnology*, **16**, 2346.

Prakash, A., McCormick, A.V., and Zachariah, M.R. 2005. Synthesis and reactivity of a super-reactive metastable intermolecular composite formulation of Al/KMnO4. *Advanced Materials (Weinheim, Germany)*, **17**, 900.

Rentz, E.J. 2003. Viral pathogens and severe acute respiratory syndrome: Oligodynamic Ag+ for direct immune intervention. *Journal of Nutritional & Environmental Medicine (Abingdon)*, **13**, 109.

Sambhy, V., MacBride, M.M., Peterson, B.R., and Sen, A. 2006. Silver bromide nanoparticle/polymer composites: Dual action tunable antimicrobial materials. *Journal of the American Chemical Society*, **128**, 9798.

Sanders, V.E., Asay, B.W., Foley, T.J., Tappan, B.C., Pacheco, A.N., and Son, S.F. 2007. Reaction propagation of four nanoscale energetic composites (Al/MoO_3, Al/WO_3, Al/CuO, and Bi_2O_3). *Journal of Propulsion and Power*, **23**, 707.

Sendroy, J. 1937. Microdetermination of chloride in biological fluids, with solid silver iodate. *J. Biol. Chem.*, **120**, 335.

Smetana, A.B., Klabunde, K.J., Marchin, G.R., and Sorensen, C.M. 2008. Biocidal activity of nanocrystalline silver powders and particles. *Langmuir*, **24**, 7457.

Son, S.F., Busse, J.R., Asay, B.W., Peterson, P.D., Mang, J.T., Bockmon, B., and Pantoya, M.L. 2002. Propagation studies of metastable intermolecular composites (MIC). *Proceedings of the International Pyrotechnics Seminar*, **29**, 203.

Stern, K.H. 2001. *High Temperature Properties and Thermal Decomposition of Inorganic Salts with Oxyanions*, CRC Press, Boca Raton, FL.

Sullivan, K.T., Young, G., and Zachariah, M.R. 2007. Enhanced reactivity of nano-B/Al/CuO MICs. *Combustion and Flame*, **156**, 302.

Sullivan, K.T., and Zachariah, M.R. 2009. Simultaneous pressure and optical measurements of nanoaluminum-based thermites: Investigating the reaction mechanism. *Journal of Propulsion and Power*, **26**, 467.

Wiberg, N., and Holleman, A.F. 2001. *Inorganic Chemistry*, Academic Press, San Diego, CA.

Zhou, L., Piekiel, N., Chowdhury, S., and Zachariah, M.R. 2009. T-Jump/time-of-flight mass spectrometry for time-resolved analysis of energetic materials. *Rapid Communications in Mass Spectrometry*, **23**, 194.